
PhysiX: A Foundation Model for Physics Simulations

Tung Nguyen*
UCLA
tungnd@cs.ucla.edu

Arsh Koneru*
UCLA
arshkon@g.ucla.edu

Shufan Li*
UCLA
jacklishufan@cs.ucla.edu

Aditya Grover
UCLA
adityag@cs.ucla.edu

Abstract

Foundation models have achieved remarkable success across video, image, and language domains. By scaling up the number of parameters and training datasets, these models acquire generalizable world knowledge and often surpass task-specific approaches. However, such progress has yet to extend to the domain of physics simulation. A primary bottleneck is data scarcity: while millions of images, videos, and textual resources are readily available on the internet, the largest physics simulation datasets contain only tens of thousands of samples. This data limitation hinders the use of large models, as overfitting becomes a major concern. As a result, physics applications typically rely on small models, which struggle with long-range prediction due to limited context understanding. Additionally, unlike images, videos, or text—which typically exhibit fixed granularity—physics datasets often vary drastically in scale, amplifying the challenges of scaling up multitask training. We introduce **PhysiX**, the first large-scale foundation model for physics simulation. PhysiX is a 4.5B parameter autoregressive generative model. It uses a discrete tokenizer to encode physical processes at different scales into a sequence of discrete tokens, and employs an autoregressive next-token prediction objective to model such processes in the token space. To mitigate the rounding error in the discretization process, PhysiX incorporates a specialized refinement module. Through extensive experiments, we show that PhysiX effectively addresses the data bottleneck, outperforming task-specific baselines under comparable settings as well as the previous absolute state-of-the-art approaches on The Well benchmark. Our results indicate that knowledge learned from natural videos can be successfully transferred to physics simulation, and that joint training across diverse simulation tasks enables synergistic learning. Code is available at <https://github.com/ArshKA/PhysiX>

1 Introduction

Simulating physical systems governed by partial differential equations (PDEs) is a cornerstone of modern science and engineering. From modeling climate and fluid dynamics to understanding galaxy formation and biological morphogenesis, PDE-based simulations enable us to predict, control, and optimize complex natural phenomena [13, 5, 6, 37, 12, 29]. Traditionally, physics simulations have relied on numerical solvers that discretize and integrate governing equations over space and time. While highly accurate, such methods are computationally intensive, often requiring specialized hardware and expert-tuned software [16]. This high cost has led to growing interest in machine learning (ML)-based surrogates, which aim to approximate simulation outputs at a fraction of

*Equal contribution.

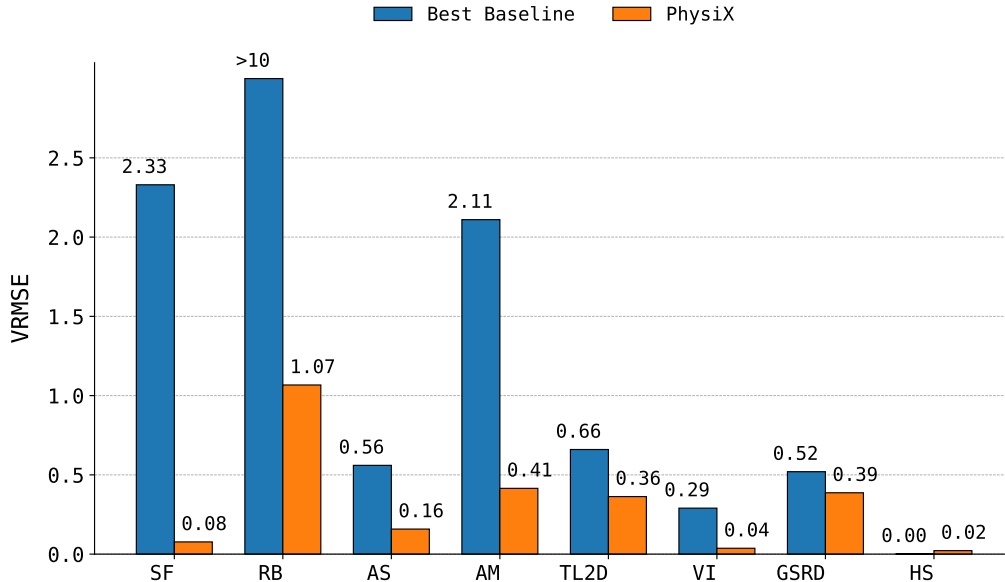


Figure 1: We propose **PhysiX**, a foundation model pretrained for physics simulations. We train PhysiX over a collection of 8 physics simulation tasks of the Well benchmark, resulting in a multi-task model that outperforms previous single-task baselines. We report VRMSE (lower is better) averaged across different physical properties and lead time between 9-26 frames for each task.

the expense [52, 55, 19]. Recent work has shown that deep neural networks can learn surrogate models for a range of PDE-driven systems, enabling orders-of-magnitude reductions in inference time [56, 49, 11, 50, 17].

Despite these promising advances, current ML-based surrogates remain largely task-specific. Most methods are designed for a single physical system and trained from scratch using individual datasets. These models typically struggle to adapt when simulation parameters change, such as domain geometry, boundary conditions, or physical constants, and often require significant retraining or architectural modification to maintain accuracy [14, 62, 38, 18]. Moreover, since they are trained separately for each task, they fail to capture shared inductive biases across domains, such as spatiotemporal locality, symmetry, or conservation laws. To address similar limitations of task-specific models in other domains, researchers have increasingly adopted the foundation model paradigm, where a large model is first pretrained on a large set of diverse data, before being finetuned for specific tasks [9, 7].

The success of foundation models raises a natural question: *can we build a foundation model for physical simulations?* Unlike text or images, physics simulations pose unique challenges. First, simulation data is expensive to generate and inherently limited in volume. Even the largest public datasets contain only tens of thousands of spatiotemporal examples [40], orders of magnitude smaller than the text or video corpora used to train large language and vision models. In addition, physical systems exhibit substantial diversity, varying in resolution, dimensionality, underlying equations, and physical domains – from turbulent fluids to elastic solids and chemical reaction-diffusion systems. Modeling such heterogeneity requires a flexible architecture and a training strategy capable of learning shared representations across domains while preserving task-specific fidelity. Together, these challenges make it non-trivial to scale the foundation model paradigm to physical simulations.

In this work, we introduce **PhysiX**, the first large-scale autoregressive foundation model for physical simulations. PhysiX comprises three main components: a universal discrete tokenizer, a 4.5B parameter autoregressive transformer, and a refinement module. We first train the tokenizer jointly on a diverse collection of physics simulation datasets to compress continuous spatiotemporal fields at different scales into sequences of discrete tokens, allowing the model to capture shared structural and dynamical patterns across domains. This discrete representation enables effective data fusion across heterogeneous sources and allows training on a unified token space analogous to language modeling. Building on this representation, we then train a large-scale autoregressive transformer

using a next-token prediction objective over the combined tokenized corpus. To further improve generalization and mitigate data scarcity, we initialize both the tokenizer and the autoregressive model from pretrained checkpoints of high-capacity video generation models, enabling PhysiX to leverage strong spatiotemporal priors learned from natural videos. Finally, to address the quantization error introduced by tokenization and improve output fidelity, PhysiX incorporates a lightweight refinement module that reconstructs fine-scale details from predicted token sequences.

Empirically, we find that PhysiX significantly outperforms task-specific baselines and previous state-of-the-art models on The Well benchmark [40], demonstrating improved long-range prediction and better generalization across tasks. Figure 1 highlights these results. Our experiments show that PhysiX can effectively transfer knowledge from natural video pretraining to physics simulations, and that joint training across multiple simulation datasets enables synergistic learning. These results demonstrate the first compelling evidence that foundation models can serve as unified surrogates for diverse physical systems, bringing us closer to general-purpose, scalable, and efficient tools for scientific computing.

2 Related Works

Physics Simulation Traditional simulation modeling typically relies on numerical methods, such as finite element methods, finite difference methods, and finite volume methods, to approximate solutions to differential equations governing physical laws. While effective, these approaches often require significant computational resources, especially for high-resolution simulations or long-term predictions, limiting their scalability and real-time applicability.

Advances in machine learning have offered promising alternatives to accelerate or supplement traditional PDE solvers [51, 22]. Physics-informed neural networks (PINNs) incorporate prior knowledge of governing equations into the loss function [46]. These methods require little observational data, as physical constraints guide the learning process. This provides the benefit of interpretable and improved physical plausibility, but makes PINNs an unsuitable choice when the underlying physical laws are unknown or only partially understood.

Concurrently, data-driven surrogate modeling methods have also seen success in this area, shifting from explicitly modeling physical laws towards implicitly learning system dynamics through observed data [34]. Early work utilized CNNs, particularly U-Net architectures [48, 63], to model spatiotemporal relationships between physical fields. More recently, neural operator frameworks have emerged, which aim to learn mappings between infinite-dimensional function spaces [28, 35]. These include Fourier Neural Operators (FNOs) [32], which leverage Fast Fourier Transforms for efficient global convolution, and various Transformer-based architectures [30, 25] that utilize attention mechanisms to capture long-range dependencies. To handle complex geometries where methods like FNOs may struggle, Graph Neural Network (GNN) based operators have also been developed, capable of operating directly on unstructured meshes [31, 8]. These operator learning frameworks enable generalization to different initial conditions, boundary conditions, and spatial resolutions without explicit retraining.

Despite these advancements, current neural network based physics simulators face limitations. They often struggle on long-range predictions [33] and many models are specialized, typically trained and optimized for a specific physical system, a narrow range of parameters, or a particular set of governing equations. Current neural network approaches are able to generalize within a given physical domain, but generally do not perform well across distinct physical domains without substantial retraining or architectural modifications.

Video Generation Video generation models have achieved considerable progress in recent years. [57, 27, 41, 2]. These models achieve high-fidelity video generation by pre-training on web-scale video data [1, 3]. The most common approach for video generation employs diffusion models [21, 4, 60], which model videos in a continuous latent space. Several works also explored autoregressive video modeling [26, 15], which convert videos into sequences of discrete tokens using a discrete tokenizer and apply the next-token prediction objective. Most notably, Emu3 [59] demonstrated that autoregressive models can achieve competitive performance when compared with diffusion models at scale. There are several dedicated lines of work focusing on specific design choices of video generative models, including video tokenizer [61, 58], model architecture [44], and learning objective [53].

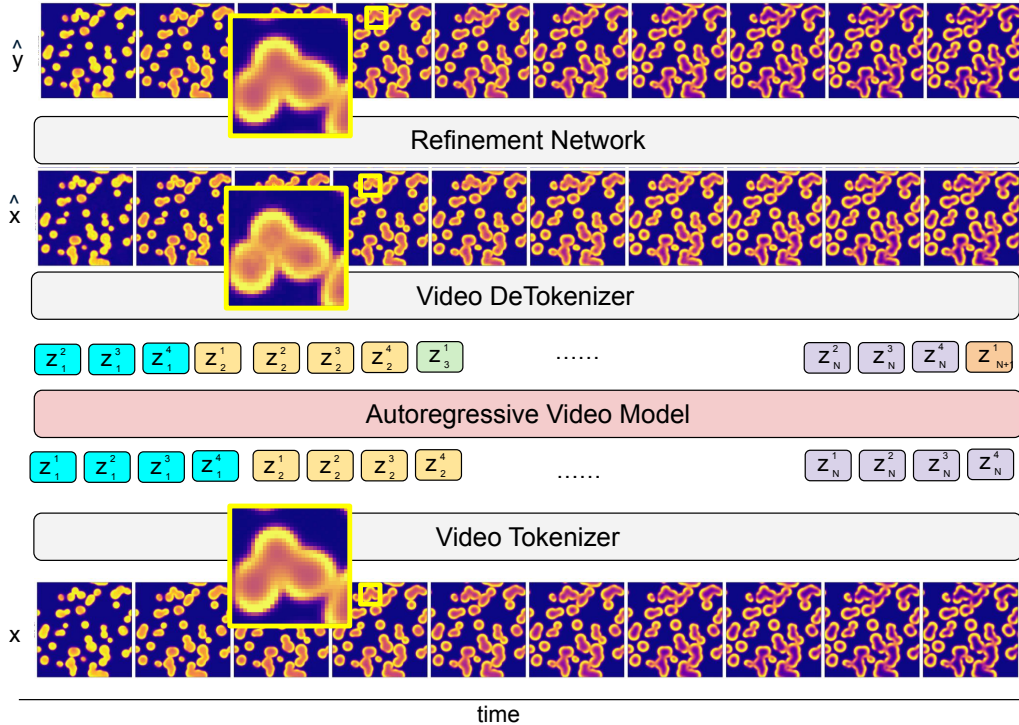


Figure 2: **The overall design of Physix.** Physix consists of a video tokenizer, an autoregressive model, and a refinement network. Given input frames x_1, \dots, x_N , the tokenizer discretizes each frame into a sequence of discrete tokens, where the j th token of frame i is denoted as $\{z_i^j\}$. The autoregressive model then generates predictions in this discrete token space, which are converted back to pixel-level predictions \hat{x} by the de-tokenizer. A refinement module is incorporated to mitigate artifacts caused by the discretization error, such as blocky, pixelated outputs (visualized in yellow boxes), and produce the final sharper and more detailed output \hat{y} .

Foundation Models The concept of foundation models first emerged in the context of transfer learning [64], where a model trained on large-scale data in one domain can be easily fine-tuned to perform many tasks in adjacent domains. Notable early examples include self-supervised learning on ImageNet-1K, a dataset of natural images [10, 20, 42]. These pre-trained vision models proved to be versatile for a wide range of downstream applications such as medical imaging [23]. More recent works shifted the training paradigm to vision-language alignment. Models like CLIP [45] are pre-trained on large amounts of image-text pairs and have demonstrated strong zero-shot generalization capabilities to a wide range of downstream tasks across multiple domains. Most recently, several works have focused on building foundation models for domain-specific use cases such as remote sensing [47], weather forecasting [39], and material design [54]. Most notably, Cosmos [2] builds a foundation world model for physical AI by pre-training on large amounts of video documenting physical applications using the video modeling objective. Its training data covers a wide range of physical applications such as robotic manipulation and self-driving. In this work, we investigate if similar approaches can be adapted to build a foundation model for physics simulations.

3 Method

Physix consists of three components: a discrete tokenizer, an autoregressive generation model, and a refinement module. Given k input frames x_1, x_2, \dots, x_k as the historical context, we first convert them into sequences of \hat{k} latent discrete tokens $z_1, z_2, \dots, z_{\hat{k}}$, where each $z_i = [z_i^1, z_i^2, \dots, z_i^L]$ consists of L tokens. We then concatenate these sequences into a single sequence, and use it as the input for the autoregressive model. The autoregressive model then predicts discrete tokens, $z_{\hat{k}+1}, z_{\hat{k}+2}, z_{\hat{k}+\hat{T}}$ where \hat{T} is the maximum lead time measured in latent frames (corresponding to

T pixel frames). These tokens are decoded back to pixel space to obtain the coarse AR prediction $\hat{x}_{k+1}, \hat{x}_{k+2}, \hat{x}_{k+T}$. We employ a refinement module to further improve the prediction. It refines \hat{x}_j , the prediction of the AR model at time step j , to obtain a refined prediction \hat{y}_j . We incorporate the refinement module as we observe that the discretization process of the tokenizer introduces small rounding errors and leads to information loss. The refinement module, which has access to the historical context in pixel space, can mitigate such error by correcting the AR predictions based on the pixel values of the context. This process is visualized in Figure 2.

3.1 Universal Tokenizer

We adopt the discrete tokenizer architecture from the Cosmos framework [2], which transforms input videos into sequences of compact discrete tokens while preserving spatiotemporal structure. The tokenizer follows an encoder-decoder design. The encoder processes an input sequence of video frames using temporally causal convolution and attention layers to produce a compressed latent representation. This representation is then quantized using Finite-Scalar Quantization (FSQ) [36], resulting in discrete token sequences. The decoder reconstructs the original video frames from these tokens. A key design choice of the Cosmos tokenizer architecture is its temporal causality, where each stage observes only past and present frames, making it well-suited for downstream autoregressive modeling. In PhysiX, we train a tokenizer with $8 \times$ spatial and $4 \times$ temporal compression. Given an input sequence of frames $x_{1:M}$, where $M = k + T$ and each frame has a size $H \times W$, the tokenizer then compresses them into $\hat{M} = \frac{k+T}{4}$ latent frames, each containing $L = \frac{HW}{8^2}$ discrete tokens. We concatenate the sequences to obtain a 1D sequence z .

To enable cross-task generalization, we train a single universal tokenizer across all available simulation datasets. This setting poses unique challenges due to the heterogeneity of the data: different datasets vary in channel dimensionality, spatial resolution, and physical semantics. We address this in two ways. First, we modify the first embedding layer of the encoder to accept a fixed union of all possible channels observed across datasets. When a data point lacks certain channels, we pad the missing entries with learnable 2D tensors specific to each channel type. This design allows the model to flexibly process any subset of channels within a unified architecture. Second, while the encoder is shared across datasets to enforce a shared embedding space, we train a separate decoder for each dataset to improve reconstruction quality and accommodate dataset-specific output distributions.

To ensure balanced representation across datasets during training, we replicate samples from datasets with fewer training examples so that each dataset contributes an equal number of sequences to the training process. We initialize the universal tokenizer from a pre-trained Cosmos checkpoint, which we found significantly accelerates convergence and improves reconstruction performance compared to training from scratch. This pre-trained initialization also facilitates better transfer to the physics domain by leveraging learned priors from natural video data.

3.2 Autoregressive Generative Models

After training the universal tokenizer, we train a large-scale autoregressive model to simulate physics in the discrete latent space. We adopt the autoregressive architecture introduced in the Cosmos framework [2], which is a decoder-only transformer trained using a next-token prediction objective. Given a sequence of discrete tokens produced by the tokenizer for the past k input frames, the transformer predicts the tokens corresponding to the next T frames autoregressively. The model minimizes the negative log-likelihood of the correct token at each position, conditioned on all previous tokens. Formally, the training objective is

$$\mathcal{L}_{\mathcal{AR}} = - \sum_{i=1}^{\hat{M}} \sum_{j=1}^L \mathbb{E}_z \left[\log p(z_i^j | \{z_m^n | m < i \text{ or } m = i, n < j\}) \right], \quad (1)$$

where $L = \frac{HW}{8^2}$ is the length of each latent frame z_i , and $\hat{M} = \frac{k+T}{4}$ since each latent frame represents four pixel frames.

The autoregressive model incorporates 3D rotary position embeddings (RoPE) to capture relative spatiotemporal relationships across the token sequence. A key distinction from prior work is our support for variable spatial resolutions during training. Since simulation datasets differ in shape, we adjust the positional encodings dynamically: rather than resizing inputs or interpolating embeddings,

we simply truncate the 3D RoPE frequencies along the height and width dimensions to match the size of the current input. This approach, implemented with minimal modification to the original RoPE module, allows seamless handling of mixed-resolution data without sacrificing performance. We found this simple strategy worked equally well as more advanced interpolation techniques [43, 65].

We initialize the autoregressive model from the 4.5B parameter Cosmos checkpoint (NVIDIA/COSMOS-1.0-AUTOREGRESSIVE-4B), enabling it to inherit strong spatiotemporal priors learned from large-scale natural video datasets. Similar to tokenizer training, we oversample smaller datasets to match the size of the largest one.

3.3 Refinement Module

The refinement module is a convolutional neural network that aims to refine the output of AR models by removing the artifacts caused by the discretization process. We show one such example in Figure 2. We observe that the output of the AR model (middle) \hat{x} exhibits a pattern that is similar to quantization noise in the center, whereas the ground truth data (bottom) x is noise-free. The refinement module is able to successfully remove such noise, as shown in its output (top) \hat{y} . This noise is introduced due to the inherent limitation of the discrete tokenization process, which was initially designed for natural videos. When generating natural videos such as characters or scenery, this noise is often negligible and does not affect the overall fidelity of generated videos. However, it can significantly hurt the performance in physical simulation tasks, where precision is required.

We train our refinement module as a post-processing step for the AR model. After the AR model is trained, we autoregressively generate predictions for each sample in the training split to produce training data for the refinement module. The ground truth frames are used as the refinement target. Notably, we decode the outputs of the AR model before passing them into the refinement model, so the model learns to improve AR generations in pixel space. We adopt the same architecture as ConvNeXt-U-Net baseline of the Well benchmark for our refinement model and utilize MSE loss during the training process. The primary difference with the baseline is the learning objective, as the refinement model learns to refine the AR output instead of predicting a new frame itself. Just as our universal tokenizer employs different decoder layers for different datasets, we train separate refinement modules for each dataset. We provide more details in the appendix.

4 Experiments

We train and evaluate PhysiX across eight simulation tasks from the Well benchmark [40], as shown in Tables 1 and 2. Following the benchmark protocol, we report the Variance-Weighted Root Mean Squared Error (VRMSE), averaged over all physical channels for each dataset. For datasets such as `helmholtz_staircase` and `acoustic_scattering (maze)`, we exclude channels that remain constant across time steps from the evaluation. We compare PhysiX against four baselines provided by the Well benchmark: Fourier Neural Operator (FNO), Tucker-Factorized FNO (TFNO), U-Net, and U-Net with ConvNeXt blocks (C-U-Net), considering both next-frame and long-horizon rollout settings.

Table 1: **Next-frame prediction performance across 8 datasets on the Well benchmark.** We report VRMSE (lower is better) averaged across different fields for each dataset.

Dataset	Baseline				Ours
	FNO	TFNO	U-Net	C-U-Net	PhysiX
<code>shear_flow</code>	1.189	1.472	3.447	0.8080	0.0700
<code>rayleigh_benard</code>	0.8395	0.6566	1.4860	0.6699	0.1470
<code>acoustic_scattering (maze)</code>	0.5062	0.5057	0.0351	0.0153	0.0960
<code>active_matter</code>	0.3691	0.3598	0.2489	0.1034	0.0904
<code>turbulent_radiative_layer_2D</code>	0.5001	0.5016	0.2418	0.1956	0.2098
<code>viscoelastic_instability</code>	0.7212	0.7102	0.4185	0.2499	0.2370
<code>gray_scott_reaction_diffusion</code>	0.1365	0.3633	0.2252	0.1761	0.0210
<code>helmholtz_staircase</code>	0.00046	0.00346	0.01931	0.02758	0.0180
Average Rank (↓)	3.62	3.75	3.62	2.38	1.62

Table 2: **Long-horizon prediction performance across 8 datasets on the Well benchmark.** We report VRMSE (lower is better) averaged across different fields for each dataset. We report averaged results over different ranges of lead time: 2-8, 9-26 and 27-56 frames.

Dataset	$\Delta t = 2:8$		$\Delta t = 9:26$		$\Delta t = 27:56$	
	Baseline	PhysiX	Baseline	PhysiX	Baseline	PhysiX
shear_flow	2.330	0.077	>10	0.153	>10	0.236
rayleigh_benard	>10	1.067	>10	0.741	>10	0.847
acoustic_scattering (maze)	0.560	0.158	0.920	1.246	1.341	2.189
active_matter	2.110	0.415	2.710	0.974	1.635	1.320
turbulent_radiative_layer_2D	0.660	0.363	1.040	0.693	1.331	0.953
gray_scott_reaction_diffusion	0.290	0.037	7.620	1.984	12.714	12.643
viscoelastic_instability	0.520	0.387	—	—	—	—
helmholtz_staircase	0.002	0.022	0.003	0.071	—	—

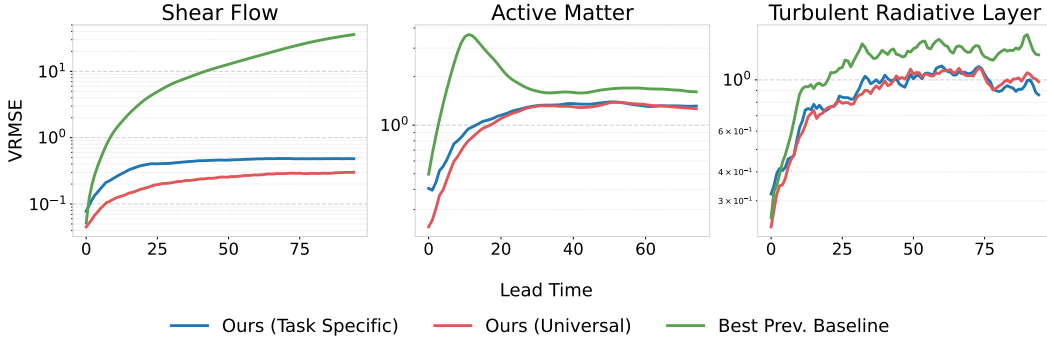


Figure 3: **Long-horizon prediction performance.** We visualize VRMSE (lower is better) across different lead time on shear_flow, active_matter, and turbulent_radiative_layer datasets.

In addition, we conduct extensive ablation studies to assess the impact of various architectural and training design choices in PhysiX.

4.1 Next-frame Prediction

In the next-frame prediction benchmark, PhysiX outperforms the baselines on 5 out of 8 datasets, demonstrating strong generalization across diverse physical systems. In addition, PhysiX achieves the best average rank across the 8 tasks, with a score of 1.62 compared to 2.38 for the best-performing baseline. Importantly, PhysiX achieves this performance using a single model checkpoint shared across all tasks, whereas the baseline results are obtained from separate models trained specifically for each dataset. This highlights the ability of PhysiX to act as a general-purpose simulator. The performance gain is especially significant on the shear_flow and rayleigh_benard datasets, where PhysiX reduces the VRMSE by 91% and 78% respectively relative to the best baseline.

4.2 Long-horizon Prediction

While PhysiX already performs competitively in next-frame prediction, its true strength lies in long-horizon simulation. As shown in Table 2, PhysiX achieves state-of-the-art performance on 18/21 evaluation points across different forecasting windows. The improvements are not only consistent but also significant in various tasks. For example, on shear_flow, PhysiX reduces VRMSE by over 97% at the 6:12 horizon compared to the best-performing baseline (from 2.33 to 0.077). On rayleigh_benard, PhysiX achieves more than 90% lower error across all rollout windows. Similar results are observed in active_matter, where PhysiX consistently achieves better performance at every forecast horizon, underscoring its robustness and adaptability across domains.

Figure 3 further illustrates the long-term behavior of PhysiX compared to the best baseline model in each dataset. In the early stages of the rollout, both models exhibit similar performance. However, as the lead time increases, the performance of the baseline models degrades rapidly due to compounding

Table 3: **Comparison of multi- and single-task models.** We report next-frame and long-horizon prediction results on the Well benchmark for the multi-task and single-task models.

Dataset	$\Delta t = 1$		$\Delta t = 2:8$		$\Delta t = 9:26$		$\Delta t = 27:56$	
	Spec.	Univ.	Spec.	Univ.	Spec.	Univ.	Spec.	Univ.
shear_flow	0.0689	0.070	0.236	0.118	0.378	0.281	0.452	0.397
rayleigh_benard	0.137	0.147	0.436	1.090	0.522	0.704	0.724	0.646
turbulent_radiative_layer	0.359	0.343	0.565	0.357	0.792	0.710	1.014	0.998
active_matter	0.150	0.090	0.844	0.477	1.177	1.396	1.352	1.381
gray_scott_reaction	0.0418	0.0210	1.487	0.0375	15.965	0.390	62.484	0.895
viscoelastic_instability	0.251	0.237	0.764	0.406	—	—	—	—

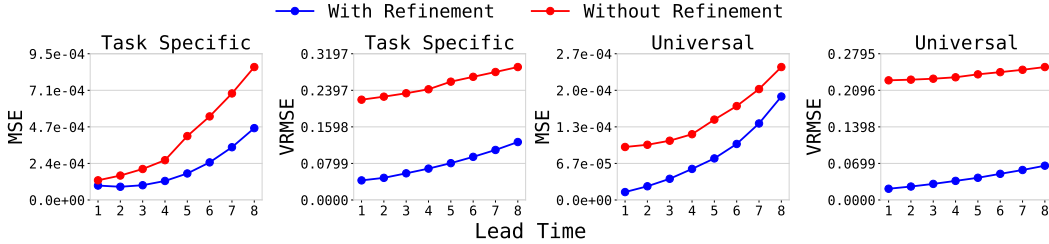


Figure 4: **Effect of refinement module.** We apply refinement module to both the multi-task and single-task AR model and study its effect on prediction errors. We report VRMSE and MSE (lower is better) over prediction windows ranging from 1 frame to 8 frames on the gray_scott_reaction_diffusion dataset.

prediction errors. In contrast, Physix maintains low VRMSE across time steps, demonstrating much greater stability. This stability stems from the autoregressive nature of Physix, which allows the model to learn from full sequences of simulations rather than focusing solely on short-term prediction. This enables it to maintain stability and accuracy over extended rollouts, making it particularly well-suited for challenging multi-step prediction tasks.

4.3 Ablation Studies

To study the effectiveness of our design, we conducted a series of thorough ablation studies. In the main paper, we explored the performance of universal (multi-task) models versus single-task models, and the effectiveness of the refinement module. We provide additional ablation studies, such as training the model from scratch versus initializing the model with weights pre-trained on natural videos in the appendix.

General Model vs Task Specific Models We compare the performance of our multi-task model and single-task models on both one-frame prediction and long-horizon prediction tasks. For the task-specific model, we followed the same setup as the universal model, including the model size, model architecture, and training hyperparameters. The only difference is the training data. We report VRMSE across 8 datasets and different lead times in Table 3. Experiment results show that the universal model outperforms task-specific models, achieving lower VRMSE on the majority of datasets across different lead times. Our results show that joint multi-task training improves the performance of individual tasks, as the model may learn some common patterns and mechanisms across different physical processes.

Effectiveness of Refinement Module We compare Physix with and without the refinement module. We show such differences for both the multi-task AR model and the single-task AR model at different prediction windows in Figure 4. The refinement model reduces MSE and VRMSE metrics for both models on all prediction windows of the gray_scott_reaction_diffusion dataset, highlighting the effectiveness of the proposed refinement process. Most notably, with the help of refinement model, the 8-frame prediction error (0.07) of our multi-task model, measured by VRMSE, is lower than the 1-frame prediction error of the best performing baseline on the Well benchmark (0.14).

Table 4: **Performance on two simulation tasks unseen during training.** We compare both the finetuning version (PhysiX_f) and the scratch version (PhysiX_s) with the baselines.

Models	euler_multi_quadrants (periodic b.c.)				acoustic_scattering (discontinuous)			
	$\Delta t = 1$	$\Delta t = 2:8$	$\Delta t = 9:26$	$\Delta t = 27:56$	$\Delta t = 1$	$\Delta t = 2:8$	$\Delta t = 9:26$	$\Delta t = 27:56$
PhysiX _f	0.105	0.188	0.358	0.642	0.038	0.057	0.443	1.168
PhysiX _s	0.105	0.188	0.366	0.658	0.039	0.062	0.455	1.192
FNO	0.408	1.130	1.370	–	0.127	2.146	2.752	3.135
TFNO	0.416	1.230	1.520	–	0.130	2.963	3.713	4.081
U-Net	0.183	1.020	1.630	–	0.045	2.855	6.259	8.074
C-U-Net	0.153	4.980	>10	–	0.006	5.160	>10	>10

4.4 Adaptation to Unseen Simulations

We evaluate the adaptability of PhysiX on two unseen simulations: `euler_multi_quadrants` (periodic b.c.) and `acoustic_scattering` (discontinuous). These tasks involve novel input channels and physical dynamics not encountered during training. To handle this distribution shift, we fully finetune the tokenizer for each task. We consider two variants of the autoregressive model: PhysiX_f, which finetunes the pretrained model, and PhysiX_s, which trains from scratch using the Cosmos checkpoint as initialization. Further finetuning details are provided in Appendix B.

Table 4 shows that PhysiX_f achieves the best performance on nearly all tasks and prediction horizons, only losing to C-U-Net on one-step prediction for one task, and the performance gap widens significantly as the horizon increases. Notably, PhysiX_f consistently outperforms PhysiX_s across all settings, highlighting its ability to effectively transfer knowledge to previously unseen simulations.

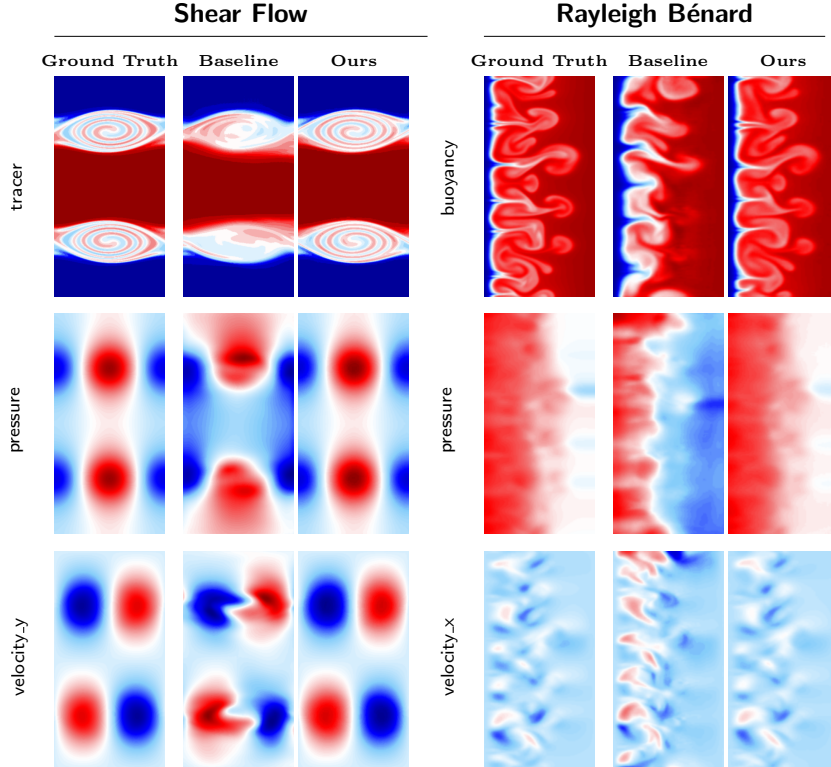


Figure 5: **Side-by-side qualitative comparison of PhysiX and baseline models.** PhysiX demonstrates superior performance in long horizon rollouts than the leading baseline model. At lead times of 24 and 15 steps for shear flow and Rayleigh–Bénard convection respectively, PhysiX maintains high-fidelity predictions across all physical fields, while baseline models ConvNeXt-UNet and TFNO exhibit visible distortions and loss of detail.

4.5 Qualitative Comparison

Figure 5 presents a qualitative comparison between PhysiX and the best-performing baseline models on two representative simulation tasks: `shear_flow` and `rayleigh_benard`. At rollout horizons of 24 and 15 steps respectively, PhysiX produces predictions that remain visually consistent with the ground truth across all physical fields, including tracer, pressure, buoyancy, and velocity components. In contrast, baseline models exhibit noticeable distortions, blurring, and loss of fine-grained structures, particularly evident in the vortex structures of `shear_flow` and the convective plumes of `rayleigh_benard`. These qualitative results highlight superior fidelity and stability of PhysiX over extended prediction windows.

5 Conclusion

PhysiX introduces a unified foundational model designed for general-purpose physical simulation across a diverse range of systems. PhysiX uses a universal tokenizer for shared discrete representations, a large-scale autoregressive transformer for modeling temporal relationships, and a refinement network to improve output fidelity. Our joint training approach enabled PhysiX to capture shared spatiotemporal patterns and adapt to varying resolutions, channel configurations, and physical semantics. We show a single universally trained model significantly outperforms task-specific baselines on a wide variety of physical domains. PhysiX demonstrates superior performance on single timestep prediction and significantly outperforms baseline methods on long-horizon rollouts, while maintaining stability and accuracy. The success of PhysiX highlights the potential of foundation models in accelerating scientific discovery by providing generalizable tools to model complex physical phenomena.

6 Acknowledgement

AG would like to acknowledge support from NSF CAREER Grant #2341040, Schmidt Sciences Early Career Fellowship, and Amazon Research Award.

References

- [1] Sami Abu-El-Haija, Nisarg Kothari, Joonseok Lee, Paul Natsev, George Toderici, Balakrishnan Varadarajan, and Sudheendra Vijayanarasimhan. Youtube-8m: A large-scale video classification benchmark. *arXiv preprint arXiv:1609.08675*, 2016.
- [2] Niket Agarwal, Arslan Ali, Maciej Bala, Yogesh Balaji, Erik Barker, Tiffany Cai, Prithvijit Chattopadhyay, Yongxin Chen, Yin Cui, Yifan Ding, et al. Cosmos world foundation model platform for physical ai. *arXiv preprint arXiv:2501.03575*, 2025.
- [3] Max Bain, Arsha Nagrani, Gül Varol, and Andrew Zisserman. Frozen in time: A joint video and image encoder for end-to-end retrieval. In *Proceedings of the IEEE/CVF international conference on computer vision*, pages 1728–1738, 2021.
- [4] Omer Bar-Tal, Hila Chefer, Omer Tov, Charles Herrmann, Roni Paiss, Shiran Zada, Ariel Ephrat, Junhua Hur, Guanghui Liu, Amit Raj, et al. Lumiere: A space-time diffusion model for video generation. In *SIGGRAPH Asia 2024 Conference Papers*, pages 1–11, 2024.
- [5] Marsha J Berger and Randall J LeVeque. Implicit adaptive mesh refinement for dispersive tsunami propagation. *SIAM Journal on Scientific Computing*, 46(4):B554–B578, 2024.
- [6] Lorenz T Biegler, Omar Ghattas, Matthias Heinkenschloss, and Bart van Bloemen Waanders. Large-scale pde-constrained optimization: an introduction. In *Large-scale PDE-constrained optimization*, pages 3–13. Springer, 2003.
- [7] Rishi Bommasani, Drew A Hudson, Ehsan Adeli, Russ Altman, Simran Arora, Sydney von Arx, Michael S Bernstein, Jeannette Bohg, Antoine Bosselut, Emma Brunskill, et al. On the opportunities and risks of foundation models. *arXiv preprint arXiv:2108.07258*, 2021.
- [8] Johannes Brandstetter, Daniel Worrall, and Max Welling. Message passing neural pde solvers. *arXiv preprint arXiv:2202.03376*, 2022.
- [9] Tom Brown, Benjamin Mann, Nick Ryder, Melanie Subbiah, Jared D Kaplan, Prafulla Dhariwal, Arvind Neelakantan, Pranav Shyam, Girish Sastry, Amanda Askell, et al. Language models are few-shot learners. *Advances in neural information processing systems*, 33:1877–1901, 2020.
- [10] Ting Chen, Simon Kornblith, Mohammad Norouzi, and Geoffrey Hinton. A simple framework for contrastive learning of visual representations. In *International conference on machine learning*, pages 1597–1607. PmLR, 2020.
- [11] Kamal Choudhary, Brian DeCost, Chi Chen, Anubhav Jain, Francesca Tavazza, Ryan Cohn, Cheol Woo Park, Alok Choudhary, Ankit Agrawal, Simon JL Billinge, et al. Recent advances and applications of deep learning methods in materials science. *npj Computational Materials*, 8(1):59, 2022.
- [12] Kyle Cranmer, Johann Brehmer, and Gilles Louppe. The frontier of simulation-based inference. *Proceedings of the National Academy of Sciences*, 117(48):30055–30062, 2020.
- [13] Veronika Eyring, Sandrine Bony, Gerald A Meehl, Catherine A Senior, Bjorn Stevens, Ronald J Stouffer, and Karl E Taylor. Overview of the coupled model intercomparison project phase 6 (cmip6) experimental design and organization. *Geoscientific Model Development*, 9(5):1937–1958, 2016.
- [14] Nicola Rares Franco, Stefania Fresca, Filippo Tombari, and Andrea Manzoni. Deep learning-based surrogate models for parametrized pdes: Handling geometric variability through graph neural networks. *Chaos: An Interdisciplinary Journal of Nonlinear Science*, 33(12), 2023.
- [15] Oran Gafni, Adam Polyak, Oron Ashual, Shelly Sheynin, Devi Parikh, and Yaniv Taigman. Make-a-scene: Scene-based text-to-image generation with human priors. In *European Conference on Computer Vision*, pages 89–106. Springer, 2022.
- [16] Jared A Goldberg, Yan-Fei Jiang, and Lars Bildsten. Numerical simulations of convective three-dimensional red supergiant envelopes. *The Astrophysical Journal*, 929(2):156, 2022.

- [17] Vignesh Gopakumar, Stanislas Pamela, Lorenzo Zanisi, Zongyi Li, Ander Gray, Daniel Brenand, Nitesh Bhatia, Gregory Stathopoulos, Matt Kusner, Marc Peter Deisenroth, et al. Plasma surrogate modelling using fourier neural operators. *Nuclear Fusion*, 64(5):056025, 2024.
- [18] Jayesh K Gupta and Johannes Brandstetter. Towards multi-spatiotemporal-scale generalized pde modeling. *arXiv preprint arXiv:2209.15616*, 2022.
- [19] Ehsan Haghghat, Maziar Raissi, Adrian Moure, Hector Gomez, and Ruben Juanes. A physics-informed deep learning framework for inversion and surrogate modeling in solid mechanics. *Computer Methods in Applied Mechanics and Engineering*, 379:113741, 2021.
- [20] Kaiming He, Haoqi Fan, Yuxin Wu, Saining Xie, and Ross Girshick. Momentum contrast for unsupervised visual representation learning. In *Proceedings of the IEEE/CVF conference on computer vision and pattern recognition*, pages 9729–9738, 2020.
- [21] Jonathan Ho, Tim Salimans, Alexey Gritsenko, William Chan, Mohammad Norouzi, and David J Fleet. Video diffusion models. *Advances in Neural Information Processing Systems*, 35:8633–8646, 2022.
- [22] George Em Karniadakis, Ioannis G Kevrekidis, Lu Lu, Paris Perdikaris, Sifan Wang, and Liu Yang. Physics-informed machine learning. *Nature Reviews Physics*, 3(6):422–440, 2021.
- [23] Hee E Kim, Alejandro Cosa-Linan, Nandhini Santhanam, Mahboubeh Jannesari, Mate E Maros, and Thomas Ganslandt. Transfer learning for medical image classification: a literature review. *BMC medical imaging*, 22(1):69, 2022.
- [24] Diederik P Kingma and Jimmy Ba. Adam: A method for stochastic optimization. *arXiv preprint arXiv:1412.6980*, 2014.
- [25] Georgios Kissas, Jacob H Seidman, Leonardo Ferreira Guilhoto, Victor M Preciado, George J Pappas, and Paris Perdikaris. Learning operators with coupled attention. *Journal of Machine Learning Research*, 23(215):1–63, 2022.
- [26] Dan Kondratyuk, Lijun Yu, Xiuye Gu, José Lezama, Jonathan Huang, Grant Schindler, Rachel Hornung, Vighnesh Birodkar, Jimmy Yan, Ming-Chang Chiu, et al. Videopoet: A large language model for zero-shot video generation. *arXiv preprint arXiv:2312.14125*, 2023.
- [27] Weijie Kong, Qi Tian, Zijian Zhang, Rox Min, Zuozhuo Dai, Jin Zhou, Jiangfeng Xiong, Xin Li, Bo Wu, Jianwei Zhang, et al. Hunyuanvideo: A systematic framework for large video generative models. *arXiv preprint arXiv:2412.03603*, 2024.
- [28] Nikola B. Kovachki, Zongyi Li, Burigede Liu, Kamyar Azizzadenesheli, Kaushik Bhattacharya, Andrew M. Stuart, and Anima Anandkumar. Neural operator: Learning maps between function spaces. *Journal of Machine Learning Research*, 24:1–97, 2023. Article 89.
- [29] Pablo Lemos, Liam Parker, ChangHoon Hahn, Shirley Ho, Michael Eickenberg, Jiamin Hou, Elena Massara, Chirag Modi, Azadeh Moradinezhad Dizgah, Bruno Regaldo-Saint Blancard, et al. Simbig: Field-level simulation-based inference of galaxy clustering. *arXiv preprint arXiv:2310.15256*, 2023.
- [30] Zijie Li, Kazem Meidani, and Amir Barati Farimani. Transformer for partial differential equations’ operator learning. *arXiv preprint arXiv:2205.13671*, 2022.
- [31] Zongyi Li, Nikola Kovachki, Kamyar Azizzadenesheli, Burigede Liu, Kaushik Bhattacharya, Andrew Stuart, and Anima Anandkumar. Neural operator: Graph kernel network for partial differential equations. *arXiv preprint arXiv:2003.03485*, 2020.
- [32] Zongyi Li, Nikola Kovachki, Kamyar Azizzadenesheli, Burigede Liu, Kaushik Bhattacharya, Andrew Stuart, and Anima Anandkumar. Fourier neural operator for parametric partial differential equations. In *International Conference on Learning Representations*. ICLR, 2021.
- [33] Phillip Lippe, Bas Veeling, Paris Perdikaris, Richard Turner, and Johannes Brandstetter. Pde-refiner: Achieving accurate long rollouts with neural pde solvers. *Advances in Neural Information Processing Systems*, 36:67398–67433, 2023.

- [34] Lu Lu, Pengzhan Jin, and George Em Karniadakis. Deeponet: Learning nonlinear operators for identifying differential equations based on the universal approximation theorem of operators. *arXiv preprint arXiv:1910.03193*, 2019.
- [35] Lu Lu, Pengzhan Jin, Guofei Pang, Zhongqiang Zhang, and George Em Karniadakis. Learning nonlinear operators via DeepONet based on the universal approximation theorem of operators. *Nature Machine Intelligence*, 3(3):218–229, 2021.
- [36] Fabian Mentzer, David Minnen, Eirikur Agustsson, and Michael Tschannen. Finite scalar quantization: Vq-vae made simple. In *The Twelfth International Conference on Learning Representations*.
- [37] Bijan Mohammadi and Olivier Pironneau. Shape optimization in fluid mechanics. *Annu. Rev. Fluid Mech.*, 36(1):255–279, 2004.
- [38] Binh Duong Nguyen, Pavlo Potapenko, Aytekin Demirci, Kishan Govind, Sébastien Bompas, and Stefan Sandfeld. Efficient surrogate models for materials science simulations: Machine learning-based prediction of microstructure properties. *Machine learning with applications*, 16:100544, 2024.
- [39] Tung Nguyen, Johannes Brandstetter, Ashish Kapoor, Jayesh K Gupta, and Aditya Grover. Climax: A foundation model for weather and climate. *arXiv preprint arXiv:2301.10343*, 2023.
- [40] Ruben Ohana, Michael McCabe, Lucas Meyer, Rudy Morel, Fruzsina Agocs, Miguel Beneitez, Marsha Berger, Blakesly Burkhart, Stuart Dalziel, Drummond Fielding, et al. The well: a large-scale collection of diverse physics simulations for machine learning. *Advances in Neural Information Processing Systems*, 37:44989–45037, 2024.
- [41] OpenAI. Sora: A video generation model. <https://openai.com/sora>, 2024. Accessed: 2025-05-13.
- [42] Maxime Oquab, Timothée Darcet, Théo Moutakanni, Huy Vo, Marc Szafraniec, Vasil Khalidov, Pierre Fernandez, Daniel Haziza, Francisco Massa, Alaaeldin El-Nouby, et al. Dinov2: Learning robust visual features without supervision. *arXiv preprint arXiv:2304.07193*, 2023.
- [43] Bowen Peng, Jeffrey Quesnelle, Honglu Fan, and Enrico Shippole. Yarn: Efficient context window extension of large language models. In *The Twelfth International Conference on Learning Representations*.
- [44] Zhiwu Qing, Shiwei Zhang, Jiayu Wang, Xiang Wang, Yujie Wei, Yingya Zhang, Changxin Gao, and Nong Sang. Hierarchical spatio-temporal decoupling for text-to-video generation. In *Proceedings of the IEEE/CVF Conference on Computer Vision and Pattern Recognition*, pages 6635–6645, 2024.
- [45] Alec Radford, Jong Wook Kim, Chris Hallacy, Aditya Ramesh, Gabriel Goh, Sandhini Agarwal, Girish Sastry, Amanda Askell, Pamela Mishkin, Jack Clark, et al. Learning transferable visual models from natural language supervision. In *International conference on machine learning*, pages 8748–8763. PmLR, 2021.
- [46] Maziar Raissi, Paris Perdikaris, and George Em Karniadakis. Physics-informed neural networks: A deep learning framework for solving forward and inverse problems involving nonlinear partial differential equations. *Journal of Computational Physics*, 378:686–707, 2019.
- [47] Colorado J Reed, Ritwik Gupta, Shufan Li, Sarah Brockman, Christopher Funk, Brian Clipp, Kurt Keutzer, Salvatore Candido, Matt Uyttendaele, and Trevor Darrell. Scale-mae: A scale-aware masked autoencoder for multiscale geospatial representation learning. In *Proceedings of the IEEE/CVF International Conference on Computer Vision*, pages 4088–4099, 2023.
- [48] Olaf Ronneberger, Philipp Fischer, and Thomas Brox. U-net: Convolutional networks for biomedical image segmentation. In *International Conference on Medical image computing and computer-assisted intervention*, pages 234–241. Springer, 2015.
- [49] Kevin Ryczko, David A Strubbe, and Isaac Tamblyn. Deep learning and density-functional theory. *Physical Review A*, 100(2):022512, 2019.

- [50] Ali Siahkoohi, Rudy Morel, Randall Balestrieri, Erwan Allys, Grégory Sainton, Taichi Kawamura, and Maarten V de Hoop. Martian time-series unraveled: A multi-scale nested approach with factorial variational autoencoders. *arXiv preprint arXiv:2305.16189*, 2023.
- [51] Shashank Subramanian, Peter Harrington, Kurt Keutzer, Wahid Bhimji, Dmitriy Morozov, Michael W. Mahoney, and Amir Gholami. Towards foundation models for scientific machine learning: Characterizing scaling and transfer behavior. In *Thirty-seventh Conference on Neural Information Processing Systems*, 2023.
- [52] Luning Sun, Han Gao, Shaowu Pan, and Jian-Xun Wang. Surrogate modeling for fluid flows based on physics-constrained deep learning without simulation data. *Computer Methods in Applied Mechanics and Engineering*, 361:112732, 2020.
- [53] Mingzhen Sun, Weining Wang, Gen Li, Jiawei Liu, Jiahui Sun, Wanquan Feng, Shanshan Lao, SiYu Zhou, Qian He, and Jing Liu. Ar-diffusion: Asynchronous video generation with auto-regressive diffusion. *arXiv preprint arXiv:2503.07418*, 2025.
- [54] Seiji Takeda, Indra Priyadarsini, Akihiro Kishimoto, Hajime Shinohara, Lisa Hamada, Hirose Masataka, Junta Fuchiwaki, and Daiju Nakano. Multi-modal foundation model for material design. In *AI for Accelerated Materials Design-NeurIPS 2023 Workshop*, 2023.
- [55] Jun Tao and Gang Sun. Application of deep learning based multi-fidelity surrogate model to robust aerodynamic design optimization. *Aerospace Science and Technology*, 92:722–737, 2019.
- [56] Giacomo Torlai, Guglielmo Mazzola, Juan Carrasquilla, Matthias Troyer, Roger Melko, and Giuseppe Carleo. Neural-network quantum state tomography. *Nature physics*, 14(5):447–450, 2018.
- [57] Ang Wang, Baole Ai, Bin Wen, Chaojie Mao, Chen-Wei Xie, Di Chen, Feiwu Yu, Haiming Zhao, Jianxiao Yang, Jianyuan Zeng, et al. Wan: Open and advanced large-scale video generative models. *arXiv preprint arXiv:2503.20314*, 2025.
- [58] Junke Wang, Yi Jiang, Zehuan Yuan, Bingyue Peng, Zuxuan Wu, and Yu-Gang Jiang. Omnitokenizer: A joint image-video tokenizer for visual generation. *Advances in Neural Information Processing Systems*, 37:28281–28295, 2024.
- [59] Xinlong Wang, Xiaosong Zhang, Zhengxiong Luo, Quan Sun, Yufeng Cui, Jinsheng Wang, Fan Zhang, Yueze Wang, Zhen Li, Qiying Yu, et al. Emu3: Next-token prediction is all you need. *arXiv preprint arXiv:2409.18869*, 2024.
- [60] Yaohui Wang, Xinyuan Chen, Xin Ma, Shangchen Zhou, Ziqi Huang, Yi Wang, Ceyuan Yang, Yinan He, Jiashuo Yu, Peiqing Yang, et al. Lavie: High-quality video generation with cascaded latent diffusion models. *International Journal of Computer Vision*, 133(5):3059–3078, 2025.
- [61] Lijun Yu, José Lezama, Nitesh B Gundavarapu, Luca Versari, Kihyuk Sohn, David Minnen, Yong Cheng, Vighnesh Birodkar, Agrim Gupta, Xiuye Gu, et al. Language model beats diffusion-tokenizer is key to visual generation. *arXiv preprint arXiv:2310.05737*, 2023.
- [62] Xiaoxuan Zhang and Krishna Garikipati. Label-free learning of elliptic partial differential equation solvers with generalizability across boundary value problems. *Computer Methods in Applied Mechanics and Engineering*, 417:116214, 2023.
- [63] Yin hao Zhu and Nicholas Zabaras. Bayesian deep convolutional encoder–decoder networks for surrogate modeling and uncertainty quantification. *Journal of Computational Physics*, 2018.
- [64] Fuzhen Zhuang, Zhiyuan Qi, Keyu Duan, Dongbo Xi, Yongchun Zhu, Hengshu Zhu, Hui Xiong, and Qing He. A comprehensive survey on transfer learning. *Proceedings of the IEEE*, 109(1):43–76, 2020.
- [65] Le Zhuo, Ruoyi Du, Han Xiao, Yangguang Li, Dongyang Liu, Rongjie Huang, Wenzhe Liu, Xiangyang Zhu, Fu-Yun Wang, Zhanyu Ma, et al. Lumina-next: Making lumina-t2x stronger and faster with next-dit. In *The Thirty-eighth Annual Conference on Neural Information Processing Systems*.

A Limitations

Despite the promising success of PhysiX, we acknowledge that it has several key limitations.

Generalization. Existing foundation models typically have zero-shot generalization capabilities. For example, CLIP [45], which was pretrained on a large set of vision-language data, can perform zero-shot classification on images for domain-specific applications. While PhysiX is trained on multiple datasets, generalizing to novel physical processes requires fine-tuning, as they may have unseen input channels or represent a drastically different dynamic system from those seen during training. We leave this to future work.

Discretization Error. The tokenization process introduces quantization errors, and while the refinement module helps mitigate this, residual errors can still affect the precision of long-term simulations. This is especially significant for datasets with low spatial or temporal variance which are much more sensitive to small perturbations. Exploring alternative tokenization schemes or end-to-end training of the tokenizer and autoregressive model could help minimize this error.

Data Diversity. PhysiX was only trained on 2D datasets, due to the architecture of the video tokenizer. This limits its direct applicability to 3D physical systems or systems with significantly different spatial structures. Future work could explore more flexible tokenization architectures that enable the compression of higher spatial dimensions, and include data from outside The Well.

B Experimental settings

Refinement Module For each trajectory in the raw training data, we randomly sample a starting timestamp and run autoregressive generation to obtain the training data for the refinement module. We adopted MSE loss. We use a global batch size of 64 frames, a learning rate of $5e - 3$ and a cosine decay learning rate scheduler. We trained each refinement model for 500 epochs on its respective data. Unlike the base model, which is trained in bfloat16 precision, we observe that using float32 precision is crucial to achieve high-quality outputs, especially for datasets with low spatial variance.

Tokenizer We trained the universal tokenizer on the 8 datasets in Table 1 for 1000 epochs with an effective batch size of 32. We optimize the models using AdamW [24] with a base learning rate of $1e - 3$, using a 10-epoch linear warmup, followed by a cosine decay schedule for the remaining 990 epochs. For model selection, we average the validation loss across all datasets after each training epoch and use the model with the lowest validation loss as the final tokenizer checkpoint.

AR Model For the autoregressive (AR) model, we trained for 10000 steps with an effective batch size of 32. We used Adam as the optimizer with a learning rate schedule similar to the tokenizer, where the number of warmup steps is set to 1000. We validated the model after every 100 training steps and used the best checkpoint for testing. For both tokenizer and AR training, we upsampled the smaller datasets to match the size of the largest one, ensuring the model learns from each dataset uniformly.

Evaluation After training, we tested the model on the held-out test set provided by the Well [40]. For the one-step setting, we evaluated the model on random sliding windows sampled from the test simulations. For the long-horizon setting, we always initiated the model from the beginning of each simulation. This adheres to the standard practice in the Well.

Finetuning To adapt PhysiX to an unseen task, we finetune both the tokenizer and the autoregressive model. Specifically, we finetune the tokenizer for 100 epochs and the autoregressive model for 1000 iterations, with similar learning rates and schedulers to pretraining. This means the compute requirement for each finetuning task is about 10% of that of pretraining. Section 4.4 shows that PhysiX was able to achieve strong performance even with this limited compute, demonstrating its usefulness for the broad research community.

C Compute resources

We trained the tokenizer and PhysiX on $8 \times 40\text{GB}$ A100 devices, and evaluated using $1 \times 40\text{GB}$ A100 device for each task. We trained PhysiX for 24 hours on $8 \times \text{A100s}$ for 8 datasets. This is approximately equal to the combined cost of training the best baseline model for each dataset at

current market rate cloud compute costs². Each model in The Well required 12 hours on $1 \times \text{H100}$ [40], for a total time of 96 H100 hours when only considering the best model for each dataset, or about half the A100 hours used by PhysiX.

D Reproducibility statement

We will release the training and evaluation code, as well as the model checkpoints. We also note that the Well’s authors³ reported some reproducibility issues with the baseline models at the moment and are planning to update the codebase and the paper. We cite the currently reported numbers in our main experiments. For numbers not reported (e.g. longer rollouts), we use the latest version of the official codebase at the time of writing.

E Licenses

Cosmos [2] is licensed under Apache-2.0, and the Well [40] benchmark follows BSD-3-Clause license. We respect the intended use of each artifact and complied with all license requirements.

F Statistical significance

While the Well does not publish variance of the baselines for test sampling, Table 5 shows that our 95% confidence interval for 1 frame prediction with PhysiX is outside the range of the baseline mean assuming a normal distribution. For rollout predictions, we start from the beginning of each sequence and evaluate on the entire test dataset, just as the baseline was evaluated.

Table 5: **PhysiX 1 frame prediction with 95% confidence intervals.**

Dataset	Interval	Dataset	Interval
shear_flow	0.070 ± 0.011	turbulent_radiative_layer	$0.210 \pm .0344$
rayleigh_benard	$0.147 \pm .029$	gray_scott_reaction	0.021 ± 0.005
acoustic_scattering (maze)	$0.096 \pm .002$	viscoelastic_instability	0.212 ± 0.029
active_matter	0.090 ± 0.011	helmholtz_staircase	0.018 ± 0.004

G Additional experiments

G.1 Pretrained vs scratch

Figure 6 compares the performance of PhysiX when initialized from a Cosmos pretrained checkpoint (Pre-trained) vs when initialized from scratch (Random). Using the pretrained checkpoint outperforms training from scratch across almost all tasks and evaluation settings, which shows the effectiveness of PhysiX in transferring prior knowledge from natural videos to physical simulations. Table 6 details the performance of the two models.

G.2 Scaling results

We study the scalability of PhysiX by training and evaluating autoregressive models with 3 different sizes: 700M, 2B, and 4B. Since Cosmos only provides the 4B model checkpoint, we initialized all 3 models in this experiment from scratch for a fair comparison. Table 7 shows that 4B is the best performing model, followed by 700M, while 2B performed the worst. We observed that both the 4B and the 2B models overfit whereas the 700M model did not, and the 2B model converged to a worse point compared to the 700M and 4B models, leading to overall poorer performances.

²Using pricing from Lambda Labs

³https://github.com/PolymathicAI/the_well/issues/49

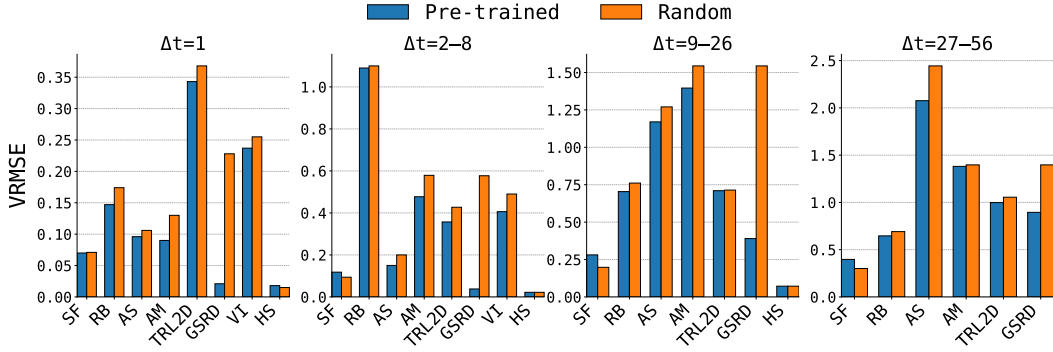


Figure 6: Comparison of pretrained and randomly initialized weights

Table 6: Comparison of pre-trained and randomly initialized models. Next-frame and long-horizon prediction results on the Well benchmark for Cosmos weights pre-trained on natural video and with randomly initialized weights.

Dataset	$\Delta t = 1$		$\Delta t = 2:8$		$\Delta t = 9:26$		$\Delta t = 27:56$	
	Pre.	Rand.	Pre.	Rand.	Pre.	Rand.	Pre.	Rand.
shear_flow	0.070	0.071	0.118	0.094	0.281	0.198	0.397	0.301
rayleigh_benard	0.147	0.174	1.090	1.100	0.704	0.761	0.646	0.691
acoustic_scattering (maze)	0.096	0.106	0.150	0.200	1.170	1.270	2.076	2.444
active_matter	0.090	0.130	0.477	0.579	1.396	1.544	1.381	1.397
turbulent_radiative_layer_2D	0.343	0.368	0.357	0.427	0.710	0.714	0.998	1.055
gray_scott_reaction_diffusion	0.021	0.228	0.038	0.577	0.390	1.544	0.895	1.397
viscoelastic_instability	0.237	0.255	0.406	0.490	—	—	—	—
helmholtz_staircase	0.018	0.015	0.022	0.022	0.072	0.072	—	—

G.3 More qualitative results

We provide additional visualizations of the Physix’s prediction results on shear_flow (Figure 7), viscoelastic_instability (Figure 8), rayleigh_benard (Figure 9) and gray_scott_reaction_diffusion (Figure 10). We compare the prediction of Physix with the ground truth and the prediction of baseline models at various lead times. Physix shows consistent improvement over baselines across all lead times. The improvements on longer lead times are more pronounced.

Table 7: **Prediction errors for Scratch models at various time horizons.** We report next-frame and long-horizon prediction errors for Scratch 4B, Scratch 2B, and Scratch 700M across different datasets, highlighting the best (lowest) error in each horizon.

Dataset	$t + 1$			$t + 2:8$			$t + 9:26$			$t + 27:56$		
	4B	2B	700M	4B	2B	700M	4B	2B	700M	4B	2B	700M
shear_flow	0.071	0.075	0.073	0.094	0.112	0.096	0.198	0.216	0.166	0.301	0.303	0.257
rayleigh_benard	0.174	0.181	0.194	1.10	1.201	1.113	0.761	0.855	0.827	0.691	0.823	0.999
acoustic_scattering (maze)	0.106	0.110	0.120	0.20	0.211	0.237	1.270	1.284	1.242	2.444	2.497	2.287
turbulent_radiative_layer	0.368	0.421	0.312	0.427	0.443	0.450	0.714	0.758	0.730	1.055	1.099	0.942
active_matter	0.130	0.102	0.105	0.579	0.592	0.623	1.544	1.626	1.394	1.397	1.415	1.417
gray_scott_reaction	0.228	0.230	0.231	0.577	0.509	0.526	1.544	1.126	1.051	1.397	2.290	1.300
viscoelastic_instability	0.255	0.319	0.246	0.490	0.494	0.590	—	—	—	—	—	—
helmholtz_staircase	0.015	0.015	0.014	0.0224	0.019	0.017	0.0718	0.056	0.061	—	—	—

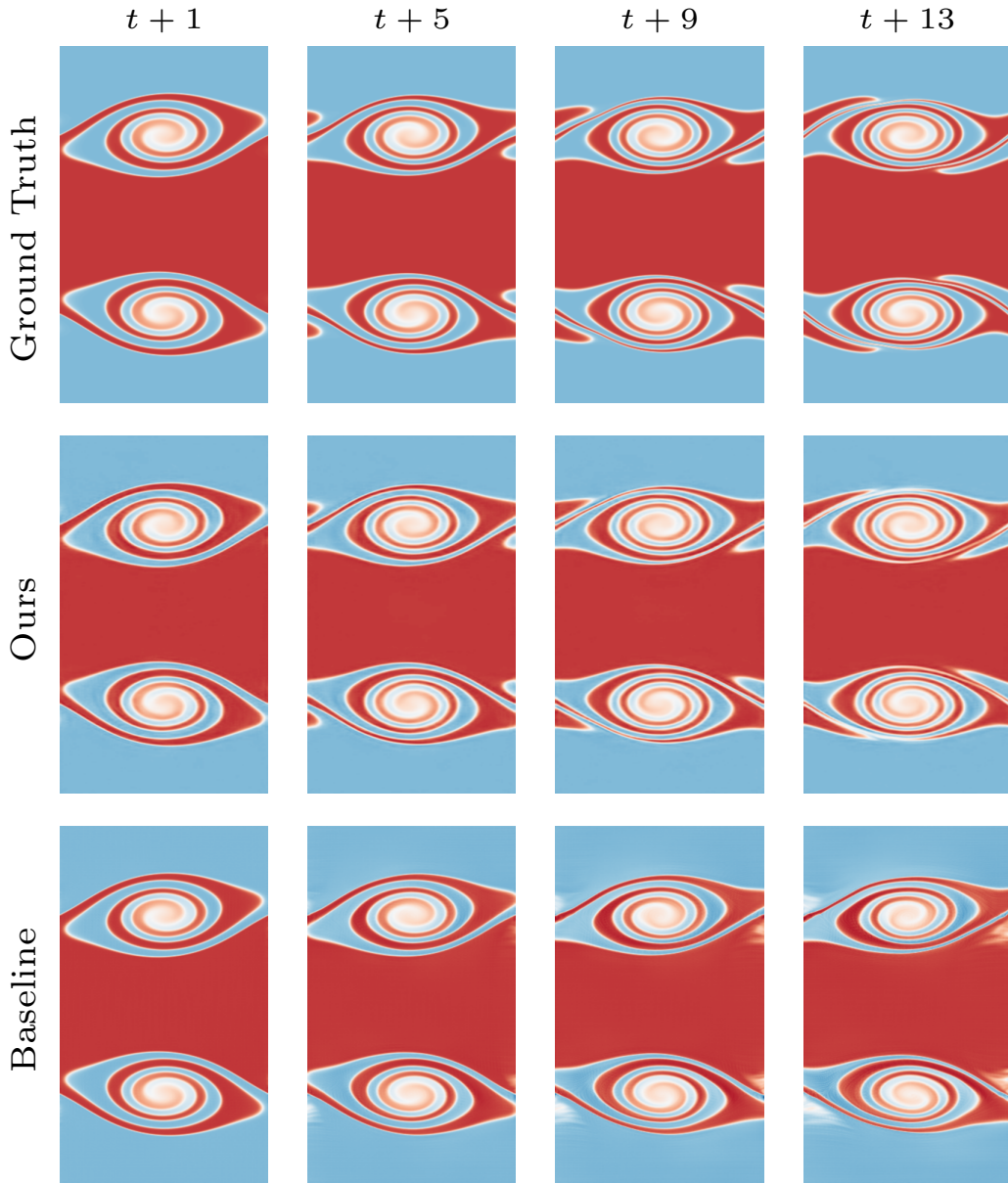


Figure 7: **Qualitative Comparisons on shear_flow Dataset.** We compare the prediction of Physix with the ground truth and the prediction of the best baseline model at lead times of 1,5,9,13 frames.

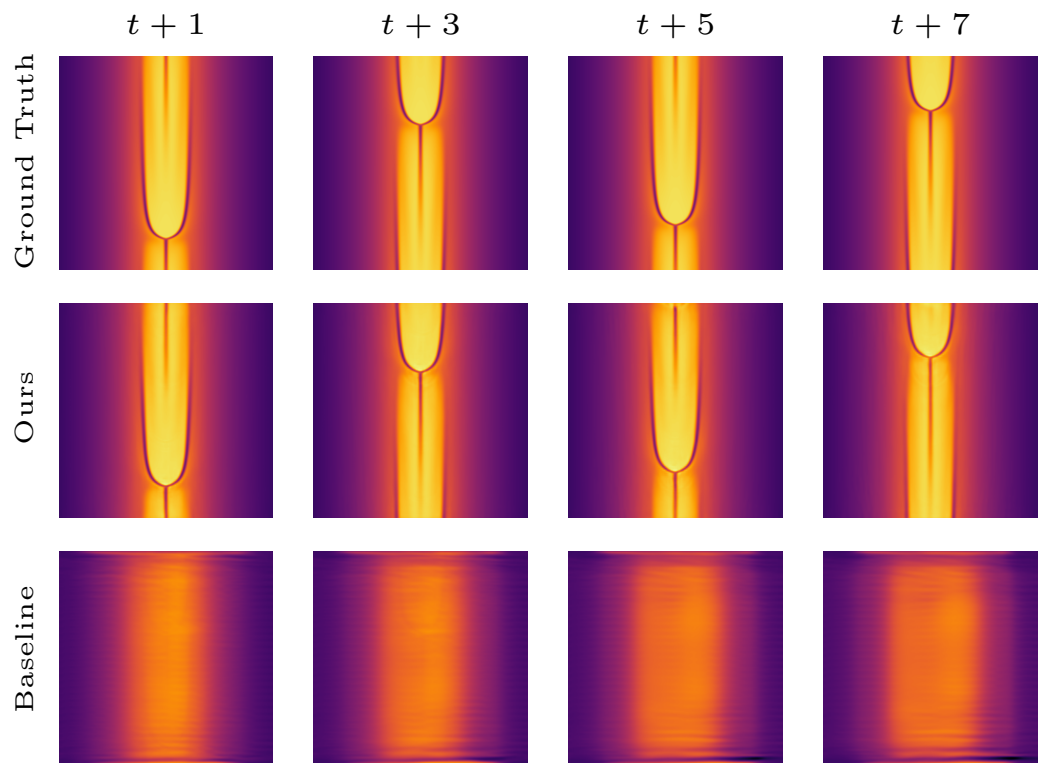


Figure 8: **Qualitative Comparisons on viscoelastic_instability Dataset.** We compare the prediction of PhysiX with the ground truth and the prediction of the best baseline model at lead times of 1,3,5,7 frames.

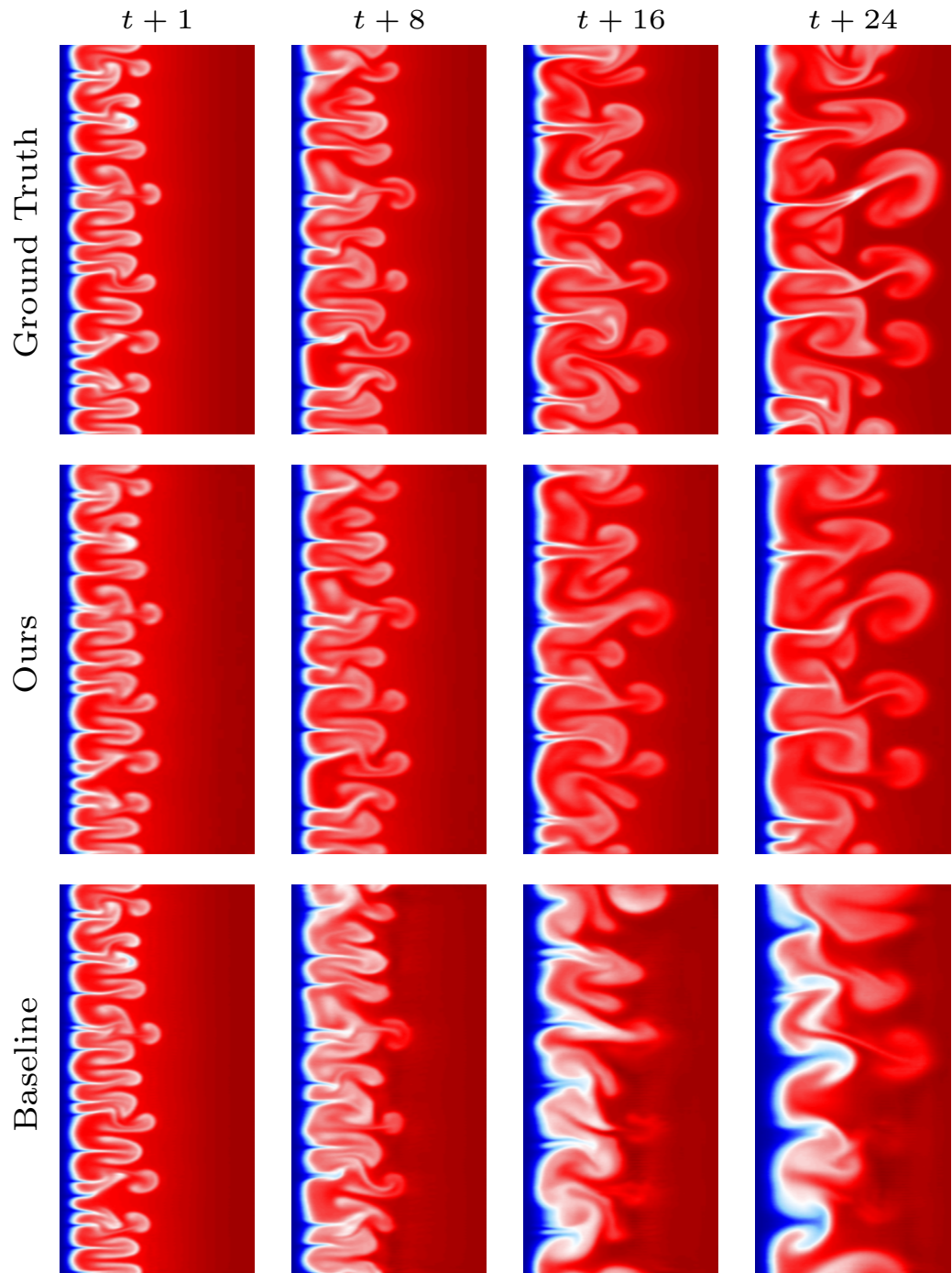


Figure 9: **Qualitative Comparisons on rayleigh_benard Dataset.** We compare the prediction of Physix with the ground truth and the prediction of the best baseline model at lead times of 1,8,16,24 frames.

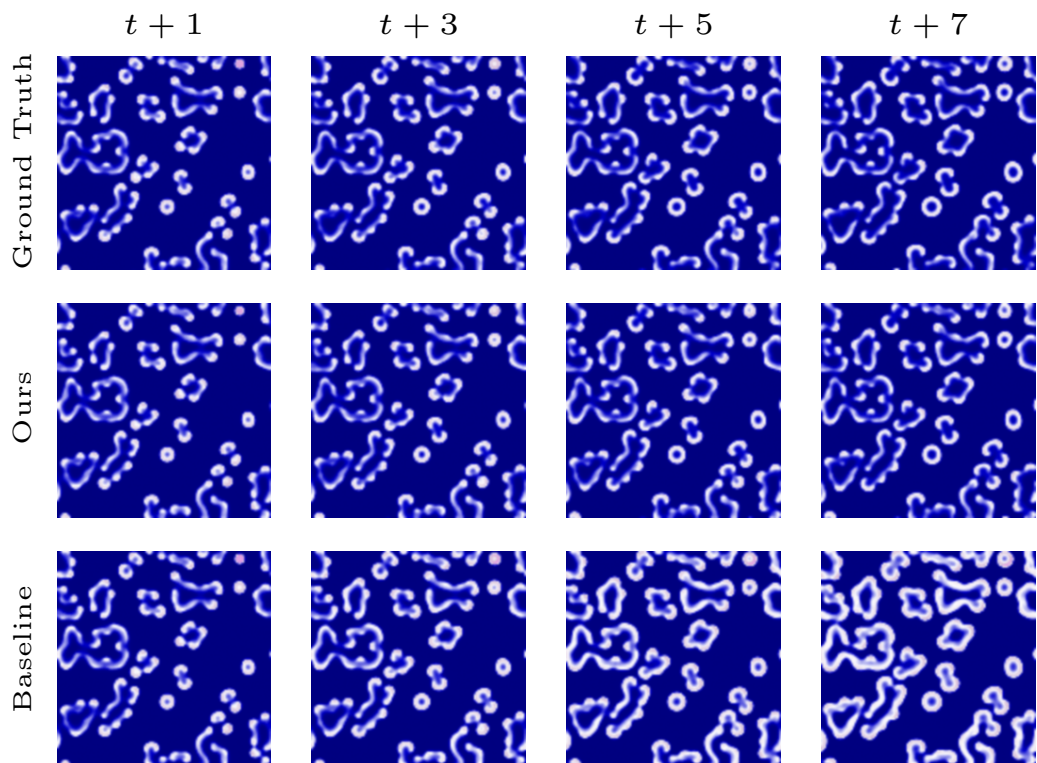


Figure 10: **Qualitative Comparisons on gray_scott_reaction_diffusion Dataset.** We compare the prediction of PhysiX with the ground truth and the prediction of the best baseline model at lead times of 1,3,5,7 frames.